JACS
JOURNAL OF THE AMERICAN CHEMICAL SOCIETY
Article
pubs.acs.org/JACS

Solid-Solutioned Homojunction Nanoplates with Disordered Lattice: A Promising Approach toward "Phonon Glass Electron Crystal" Thermoelectric Materials

Chong Xiao,[†] Jie Xu,[†] Boxiao Cao,[†] Kun Li,[†] Mingguang Kong,[‡] and Yi Xie*[,†]

[†]Hefei National Laboratory for Physical Sciences at the Microscale, University of Science & Technology of China, Hefei, Anhui 230026, P.R. China

[‡]Key Laboratory of Materials Physics, Institute of Solid State Physics, Chinese Academy of Science, Hefei, Anhui 230031, P.R. China

Supporting Information

ABSTRACT: The concept of "phonon glass electron crystal" (PGEC) was proposed in the mid-1990s to maximize the *ZT* value for thermoelectric materials, based on its combined advantages of low thermal conductivity as in a glass but high electricity as in a well-ordered crystal. Although a great amount of research in complex materials systems for achieving this concept has been done, a perfect "PGEC" material has not been acquired yet. Herein, we first put forward a solid-solutioned homojunction in high temperature phase with disordered lattice, which possesses both high electrical conductivity and low thermal conductivity, as an effective way to optimize the low/mid-temperature thermoelectric property. As an example, nonambient cubic phase $AgBiSe_2$ was successfully stabilized to room temperature through the formation of a solid solution by Sb incorporation for the first time, and furthermore, in situ formed homojunctions on the surface of solid-solutioned nanoplates were also first achieved through a simple colloidal method. A significant enhancement of thermoelectric performance at low/mid-temperature was realized through synergistical regulation on electronic and thermal transport. As a result, compared to that of original $AgBiSe_2$ (ZT = 0.03 at 550 K), the ZT value of $AgBi_{0.5}Sb_{0.5}Se_2$ was increased to 0.51 at 550 K by the formation of a solid solution, and then further increased to 1.07 at 550 K by the formation of solid-solutioned homojunction.

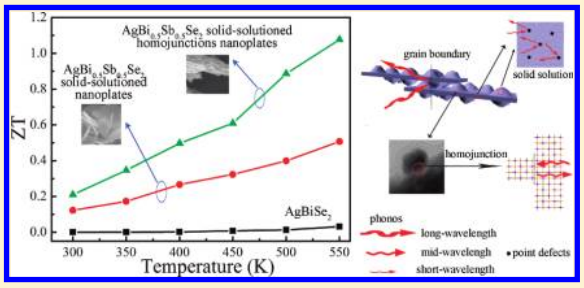

INTRODUCTION

Thermoelectric materials have attracted tremendous attention because of their capability to directly create electricity from waste heat sources.[1−4] The performance of thermoelectric materials is quantified by a dimensionless figure of merit, ZT, which is defined as $\sigma S^2T/\kappa$, where σ is the electrical conductivity, S is the Seebeck coefficient, κ is the thermal conductivity, and T is the absolute temperature. A good thermoelectric material should be a perfect combination of high power factor (σS^2) with low thermal conductivity. However, there is a strong correlation of these three parameters according to the Wiedemann−Franz law.[5] As known, the thermal conductivity (κ) is the sum of two independent components, a lattice contribution κ_l and an electronic contribution κ_e equal to $L\sigma T$ according to the Wiedemann−Franz law. According to the Wiedemann−Franz law, only the lattice contribution to the thermal conductivity, κ_l, is independent of the electrical conductivity. Therefore, in order to further improve the figure of merit, progress in enhancing the ZT values by substantial reduction of lattice thermal conductivity is highly desirable.

In the mid-1990s, an intriguing idea to achieve maximum ZT was proposed by Slack and is referred as the "phonon glass electron crystal" (PGEC) approach,[6] which idealistically behaves as a glass with respect to phonon scattering (low thermal conductivity) and as a crystal with respect to electron scattering (high electrical conductivity). Although a significant amount of research in complex materials systems such as Skutterudites,[7] Zintl phases,[8] and Clathrates[9] has been done, a perfect "PGEC" material has not been acquired yet.[10] Beyond these traditional materials, those materials with disordered structure may be other candidates for the "PGEC" concept, such as I−V−VI_2 compounds. Previous theoretical calculations[11] showed that the atom disordering in the lattice could cause much stronger anharmonicity of the chemical bond, which drives the phonon−phonon umklapp and normal scattering processes that could intrinsically limit the lattice thermal conductivity, and simultaneously show high electrical conductivity due the high mobility of these disordering ions.

$AgBiSe_2$, as a typical member of I−V−VI_2 compounds, attracts our interest thanks to the disordering of Ag and Bi ions in the lattice, which may create its intrinsic high conductivity and low thermal conductivity characteristics.[11] At room temperature, $AgBiSe_2$ is a *p*-type semiconductor and crystallizes in the hexagonal phase, and is observed to undergo a structural phase transition from a high temperature (T > 560 K) cubic

Received: March 8, 2012
Published: April 23, 2012

dx.doi.org/10.1021/ja3020204 | J. Am. Chem. Soc. 2012, 134, 7971−7977

phase to an intermediate temperature (393 K < T < 560 K) rhombohedral structure and then to a low temperature (T < 393 K) hexagonal phase with temperature decreasing,[12,13] as schematically shown in Figure 1. The intermediate temperature

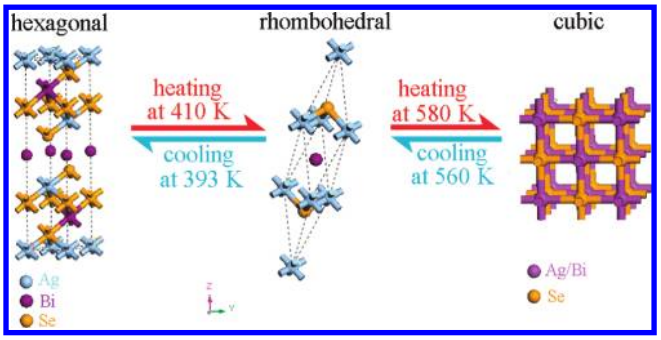

Figure 1. Schematic representation of the structure phase transition between hexagonal, rhombohedral, and cubic $AgBiSe_2$.

phase has a rhombohedral structure belonging in space group $R\bar{3}m$ with lattice constants a = 7.022 Å and α = 34.5°,[12] in which the ordering of Ag and Bi ions takes place in quite distinguishable positions. The low temperature phase has a hexagonal cell of space group $P\bar{3}m1$, with parameters a = 4.18 Å and c = 19.67 Å.[12] Both low temperature hexagonal and intermediate temperature rhombohedral phase $AgBiSe_2$ are narrow-band gap semiconductors, while only the high-temperature cubic phase is regarded to behave as metallic in electrical conductivity with low thermal conductivity, because of the disordered arrangements of the Ag and Bi atoms in the lattice. In other words, the cubic $AgBiSe_2$ with intrinsic high electrical conductivity and low thermal conductivity could only be achieved at high temperature, which is too high to settle for the current development of low-temperature thermoelectric materials for solar thermal energy direct conversion.[14−16] Therefore, stabilization of the high temperature phase $AgBiSe_2$ (crystallizes in the cubic phase) to room temperature should be desirable for broadening the working temperature range as an excellent thermoelectric material.

As known, thermal transport in solids is the dissipation of vibrational energy between adjacent atoms through chemical bonds.[17] In the quantum theory, it is considered as the energy transfer between phonons. That is to say, the lattice thermal conductivity (κ_l) is the result of movement by heat carrying phonons through the lattice. Therefore, to increase the phonon scattering becomes the key to reduce the lattice thermal conductivity. It is believed that the formation of solid solution is an effective way of reducing the lattice thermal conductivity via point defect scattering of phonons.[10] Point defect scattering serves to decrease the lattice thermal conductivity by increasing the frequency and magnitude of the scattering events for the heat carrying phonons. However, while the significant reduction of lattice thermal conductivity can be achieved in solid solution, there is often a concurrent deterioration in electronic performance because of the reduction in the charge carrier mobility, thus limiting the overall ZT enhancement.[10] Therefore, how to minimize the thermal conductivity with no deteriorated electrical conductivity for improving thermoelectric properties is still challenging. At the same time, transition temperature of inorganic materials with phase transition behavior can also be altered by the formation of solid solution. For example, by incorporation of molybdenum into the VO_2 lattice, the phase transition temperature from insulator monoclinic phase to metallic rutile phase could be suppressed to room temperature.[18] Also, our group have realized the stabilization of nonambient rutile VO_2 to room temperature by hydrogen incorporation, in which carrier concentration can be simultaneously adjusted to improve thermoelectric properties.[19] Therefore, stabilization of nonambient $AgBiSe_2$ with disordered lattice to room temperature through the formation of solid solution seems to be rational and interesting not only for simultaneously possessing high electrical conductivity and low thermal conductivity in a wide temperature range, which conform the concept of "PGEC" approach, but also for overcoming the disadvantages of deteriorated electrical conductivity in conventional solid solution.

As another effective strategy for reduction of thermal conductivity, significant effort has been devoted to heterostructures in the recent research about the nanostructure-based thermoelectric materials.[20] Theoretically, an enhancement of the power factor could potentially realize the suppression of the thermal conductivity by interface scattering of phonons. However, the heterogeneous composition in heterojunctions seems to be adverse for the high electrical conductivity due to the scattering of electrons at the heterointerface. Different from heterojunctions, homojunctions are constructed with the same building blocks of nanoscale dimensions, but also can provide a lot of interface similar to heterojunctions for the reduction of thermal conductivity. Moreover, the homojunction, with homogeneous composition, seems to be favorable for the reduction of thermal conductivity with no deteriorated electrical conductivity than heterojunctions. However, investigation of thermoelectric properties with homojunctions has been long neglected.

Herein, we first put forward that the solid-soltioned homojunction nanostructures in high temperature phase with disordered lattice as an effective way to optimize the low/mid-temperature thermoelectric property. As an example, nonambient $AgBiSe_2$ phase to room temperature successfully stabilized to room temperature through the formation of solid solution by Sb substitution for the first time. Furthermore, in situ formed solid-solutioned homojunction nanoplates were also successfully synthesized through a simple colloidal method for the first time. We highlight that the formation of solid solution and homojunction synergistically much enhanced the thermoelectric properties. As expected, because of the stabilization of high temperature phase to room temperature by the formation of solid solution with the incorporation of Sb into the lattice, the intrinsic high electrical conductivity and low thermal conductivity were obtained at a whole temperature range, which were only obtained at high temperature previously. As a result, compared to that of original $AgBiSe_2$ (ZT = 0.03 at 550 K), the ZT value of $AgBi_{0.5}Sb_{0.5}Se_2$ solid-solutioned nanoplates was increased to 0.51 at 550 K. Moreover, the ZT value of solid-solutioned homojunction $AgBi_{0.5}Sb_{0.5}Se_2$ nanoplates was further increased to 1.07 at 550 K, which is due to the further reduction of thermal conductivity with no deteriorated electrical conductivity by the introduction of a rough surface on the solid-solutioned nanoplates.

■ EXPERIMENTAL SECTION

Materials. All chemicals were of analytic grade purity obtained from Sinopharm Chemical Reagent Co., Ltd. and used as received without further purification.

Synthesis of $AgBi_{1-x}Sb_xSe_2$ Solid-Solutioned Nanoplates. In this study, we have synthesized a series of $AgBi_{1-x}Sb_xSe_2$ (x = 0, 0.25, 0.5, 0.75, and 1) solid-solutioned nanoplates. Taking $AgBi_{0.5}Sb_{0.5}Se_2$ as an example, first, a Bi(III)-complex and Sb(III)-complex precursor solution was prepared by adding 0.193 g of bismuth acetate and 0.149 g of antimony acetate to 2 mLof 2-ethylhexanoic acid in a flask, respectively. The mixture was kept at 80 °C and stirred for 30 min until a uniform mixture was formed and then cooled to room temperature. Second, selenium precursor solution was prepared in a separate flask, where 0.2 g of Se powder was mixed with 20 mL of oleylamine, kept at 180 °C, and then stirred for 30 min. Third, Bi(III)-complex and Sb(III)-complex precursor solution was swiftly injected into the Se-precursor solution, and 0.170 g of $AgNO_3$ also was added into the Se-precursor solution. The mixture was maintained at 180 °C for 3 h under stirring, and then the reaction was quickly stopped. The nanoplates were separated from the resulting solution by centrifuge and washed for several times with ethanol and cyclohexane. All the samples were dried in a vacuum at 60 °C for 6 h.

Synthesis of $AgBi_{0.5}Sb_{0.5}Se_2$ Solid-Solutioned Homojunction Nanoplates. In a typical synthesis of $AgBi_{0.5}Sb_{0.5}Se_2$ homojunction nanoplates, 0.193 g of bismuth acetate and 0.149 g of antimony acetate were added into 20 mL of oleylamine and kept at 80 °C under stirring for 30 min. Then 0.2 g of Se powder was added into the mixture after the mixture was heated up to 180 °C. The mixture was maintained at 180 °C for 1 h under stirring, and then 0.170 g of $AgNO_3$ was added. After the mixture was maintained at 180 °C for 1 h under stirring, the reaction was quickly stopped. The samples were separated from the resulting solution by centrifuge and washed for several times with ethanol and cyclohexane. All the samples were dried in a vacuum at 60 °C for 6 h.

Surfactant Removal Process and Bulk Samples Preparation. The organic surfactants were removed via the procedure of a previous report[21] before fabrication of bulk samples for thermoelectric measurement. Briefly, as-prepared silver chalcogenides were dispersed in cyclohexane with hydrazine solution (85% v/v) and stirred vigorously until all the nanocrystals were precipitated. The supernatant was decanted, and the precipitate was washed with ethanol three for times to remove hydrazine and collected by centrifugation, and then dried in vacuum at 65 °C. After the hydrazine treatment, the nanocrystals were hot-pressed into rectangular (10 mm × 4 mm × 1.5 mm) and round disk bulk samples (with diameter of about 13 mm and thickness of 2 mm) under 60 MPa at 400 °C for 30 min.

Characterization. The structure of these obtained samples was characterized via X-ray diffraction (XRD) pattern, which was recorded on a Rigaku Dmax diffraction system using a Cu Kα source (λ = 1.54187 Å). X-ray photoelectron spectroscopy (XPS) measurements were performed on a VGESCALAB MK II X-ray photoelectron spectrometer with an excitation source of Mg Kα = 1253.6 eV. The field emission scanning electron microscopy (FESEM) images were taken on a JEOL JSM-6700F scanning electron microscope. High-resolution transmission electron microscopy (HRTEM) images were performed on a JEOL-2010 transmission electron microscope at 200 kV.

Thermoelectric Properties. Rectangular shape samples with typical sizes of 10 mm × 4 mm × 1.5 mm were employed to simultaneously measure electrical conductivity σ and Seebeck coefficient S by the standard four-probe methods in a He atmosphere (ULVAC-RIKO ZEM-3). Thermal conductivity κ was calculated using the equation $\kappa = a\rho C_p$ from the thermal diffusivity a obtained by a flash diffusivity method (LFA 457, Netzsch) on a round disk sample with diameter of about 13 mm and thickness of 2 mm, and specific heat C_p determined by a differential scanning calorimeter method (DSC Q2000, Netzsch).

RESULTS AND DISCUSSION

It is well-known that one of the principal features of semiconductor thermoelectrics is a high electrical conductivity and low lattice thermal conductivity. The most extraordinary aspect of the high temperature phase $AgBiSe_2$ with cubic structure should possess comparably high electrical conductivity and very low lattice thermal conductivity that they exhibit, as predicted by theoretical calculations. Previously, the density functional theoretical calculations[13] suggested that $AgBiSe_2$ could crystallize in cubic phase at high temperature, which has Ag and Bi disordering, and might be metallic with comparably high electrical conductivity. Theoretical calculations also implied that the lattice thermal conductivity of $AgBiSe_2$ is limited to its minimum possible value by intrinsic phonon−phonon scattering processes.[11] However, the high electrical conductivity and intrinsic low thermal conductivity were only expected in the high temperature phase of $AgBiSe_2$ with cubic structure. Inspired by the above analysis, we attempt to stabilize the nonambient $AgBiSe_2$ to room temperature through the formation of solid solution by Sb substitution, because of the similar valency, electronegativities, atomic radii, and crystal structure of Sb compared to those of Bi.

Solid-solutioned $AgBi_{1-x}Sb_xSe_2$ nanoplates were synthesized under a simple colloidal method. The crystalline phase and crystallinity of the as-synthesized samples were well characterized by X-ray diffraction (XRD). As shown in Figure 2a,

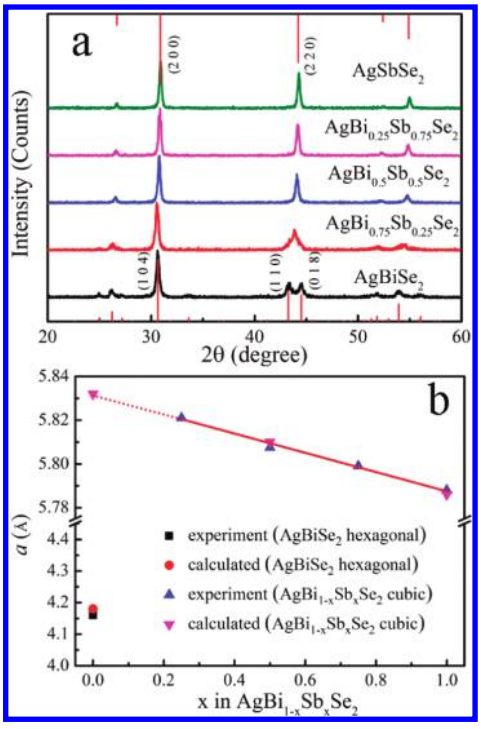

Figure 2. (a) XRD patterns of $AgBi_{1-x}Sb_xSe_2$ solid solution samples. (b) Variation of the cell parameters (refined from the power patterns) with the Sb content (x).

without Sb doping (x = 0), the XRD patterns match well with the standard hexagonal $AgBiSe_2$ (space group: $P\bar{3}m1$) with lattice constants a = 4.18 Å and c = 19.67 Å (JCPDS 74-0842). While the Sb absolutely substitutes Bi (x = 1), the product can be indexed to cubic $AgSbSe_2$ (space group: $Fm\bar{3}m$) with lattice parameters of a = 5.786 Å (JCPDS 89-3670). No other peaks can be detected, indicating the high purity of the samples. In the case of the $AgBi_{1-x}Sb_xSe_2$ solid solutions, the combination of the $AgBiSe_2$ (110) and (018) peaks into a (220) peak indicates the stabilization of the high temperature cubic phase of $AgBiSe_2$ to room temperature through the formation of solid solution by incorporation of Sb. Lattice parameters for the

dx.doi.org/10.1021/ja3020204 | J. Am. Chem. Soc. 2012, 134, 7971−7977

$AgBi_{1-x}Sb_xSe_2$ ($0 \le x \le 1$) nanoplates were calculated. As smaller Sb^{3+} cations are introduced into the solid solution, the unit cell undergoes a systematic decrease in lattice parameter, as demonstrated by the shift of the peaks of the patterns to higher 2θ values (Figure 2a). This gradual shift indicates a homogeneous distribution of cations, forming a single phase of solid solution as opposed to a mixture containing domains of both $AgBiSe_2$ and $AgSbSe_2$. Furthermore, the refined lattice parameters (Figure 2b) showed almost linear contraction with increasing Sb content, which accords well with Vegard's law, which indicates the isomorphic substitution in the cation positions of larger Bi by smaller Sb atoms.

It is well-known that X-ray photoelectron spectroscopy (XPS) is a very useful method in determination of the chemical compositions, and the as-obtained products were also analyzed by XPS. The survey spectra of XPS (as shown in Figure S1 in the Supporting Information) indicate the presence of Ag, Bi, Sb, and Se in the samples, where the presence or absence of Bi and Sb depends on the x value in $AgBi_{1-x}Sb_xSe_2$. The binding energies of Ag $3d_{3/2}$ and Ag $3d_{5/2}$ are located at 373.6 and 367.5 eV (Figure 3a) with a peak splitting of 6.1 eV which was

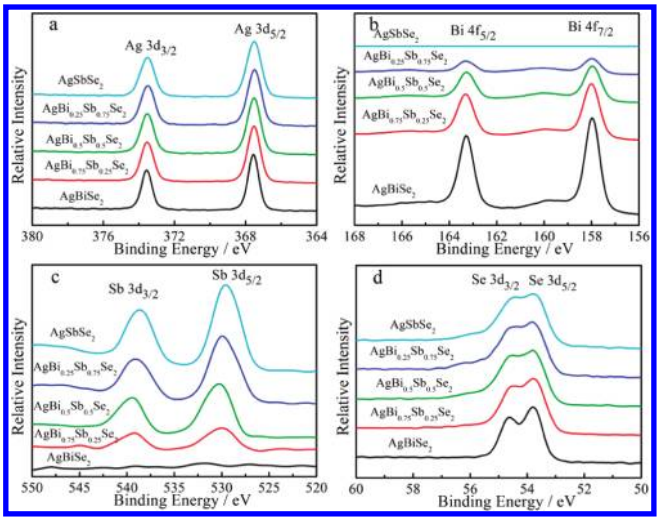

Figure 3. XPS spectra of the solid-solutioned $AgBi_{1-x}Sb_xSe_2$ nanoplates. (a) Ag spectra, (b) Bi spectra, (c) Sb spectra, and (d) Se spectra.

consistent with the standard reference XPS spectrum of Ag(I). The two strong peaks at 157.9 and 163.3 eV (Figure 3b) can be attributed to Bi $4f_{7/2}$ and Bi $4f_{5/2}$, respectively. The peaks at 538.6 and 529.7 eV (Figure 3c) reveal Sb $3d_{3/2}$ and Sb $3d_{5/2}$, respectively. The peaks at 53.8 and 54.6 eV (Figure 3d) can be assigned to the Se $3d_{5/2}$ and Se $3d_{3/2}$, respectively. It is evident that the amount of Bi gradually decreases while that of Sb systematically increases with increasing x values in this series of samples. No peaks of other elements are observed in the wide XPS survey spectrum, indicating the high purity of the $AgBi_{1-x}Sb_xSe_2$ products.

The morphology and size of the as-prepared samples are studied by FESEM. The low-magnification FESEM image of $AgBi_{0.5}Sb_{0.5}Se_2$ (see Figure S2b in the Supporting Information) reveals that a large number of platelike nanostructures are randomly dispersed on the surface of the substrate. A high-magnification FESEM image (Figure 4a) shows that the edge length of the plates is in the range of 400–600 nm, and that their thickness is quite thin, about 25 nm. To further investigate

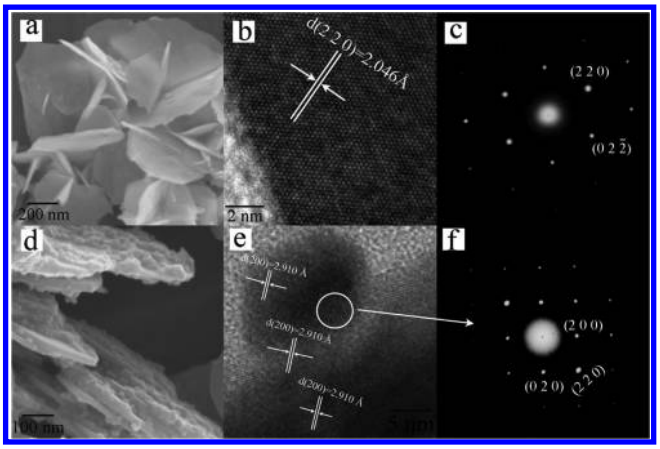

Figure 4. High-magnification FESEM images, HRTEM images, and SAED patterns for $AgBi_{0.5}Sb_{0.5}Se_2$ solid-solutioned nanoplates (a–c) and $AgBi_{0.5}Sb_{0.5}Se_2$ solid-solutioned homojunction nanoplates (d–f), respectively.

the microstructural details of the $AgBi_{0.5}Sb_{0.5}Se_2$ platelike nanostructures, HRTEM and SAED analysis were carried out. A representative HRTEM image of the edge area of the $AgBi_{0.5}Sb_{0.5}Se_2$ solid-solutioned nanoplate in Figure 4b exhibits well-resolved 2D lattice fringes and shows that the nanoplate is a well-crystallized single crystal. The plane spacings of 2.046 Å correspond to the lattice planes of (220). The selected-area electron diffraction (SAED) taken from the edge of this nanoplate in Figure 4c further confirms the single-crystal nature of the nanoplates.

For the thermoelectric properties measurements, we have carefully removed the organic surfactants according to the procedures of previous report[21] and fabricated the hot-pressed bulk samples. Taking $AgBi_{0.5}Sb_{0.5}Se_2$ solid-solutioned nanoplates as an example, the XRD patterns and SEM images of surface cleaned and hot-pressed bulk samples are shown in Figure S2. As shown in Figure S2a, there are no apparent changes of structure and purity of the samples was detected after hydrazine treatment and hot-pressing compared to the pristine nanocrystals. The SEM image (Figure S2b and c) of solid-solutioned nanoplates clearly shows that the size and shape were almost unchanged after hydrazine treatment, and also the bulk sample consisting of hot-pressed solid-solutioned nanoplates were very dense (Figure S3d). The temperature dependence of thermoelectric properties for $AgBiSe_2$ and $AgBi_{0.5}Sb_{0.5}Se_2$ is measured and shown in Figure 5. As shown in Figure 5a, regardless of composition, the positive sign of the Seebeck coefficients indicates that both $AgBiSe_2$ and $AgBi_{0.5}Sb_{0.5}Se_2$ nanoplates are both p-type semiconductors. Although at ambient temperature the two samples have comparable Seebeck coefficients, distinctly different trends in the temperature dependence of the Seebeck coefficient divide the samples into two groups: with the increasing temperature, the Seebeck coefficient of $AgBiSe_2$ initially increases, reaches a maximum, and then decreases to a value approaching that of solid-solutioned $AgBi_{0.5}Sb_{0.5}Se_2$ nanoplates. In contrast, the Seebeck coefficient of $AgBi_{0.5}Sb_{0.5}Se_2$ solid-solutioned nanoplates monotonically decrease with the increasing temperature. The two different trends also reveal the successful stabilization of solid-solutioned $AgBiSe_2$ with cubic structure to room temperature by incorporation of Sb, while the abrupt change of Seebeck coefficient between 420 and 500 K in $AgBiSe_2$ was in

dx.doi.org/10.1021/ja3020204 | J. Am. Chem. Soc. 2012, 134, 7971–7977

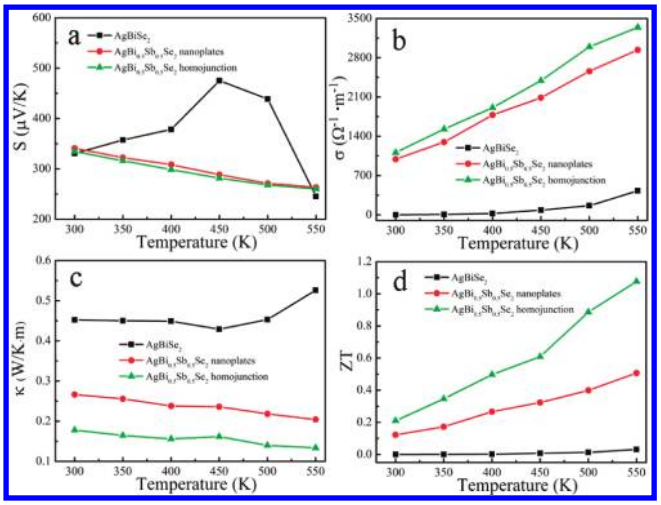

Figure 5. Temperature-dependence of the Seebeck coefficient (a), electrical conductivity (b), thermal conductivity (c), and thermoelectric figure of merit ZT (d) for $AgBiSe_2$ nanoplates, $AgBi_{0.5}Sb_{0.5}Se_2$ solid-solutioned nanoplates, and $AgBi_{0.5}Sb_{0.5}Se_2$ solid-solutioned homojunction nanoplates, respectively.

fact contributed by the structural phase transition from hexagonal phase to rhombohedral phase.

Figure 5b shows the temperature dependence of electrical conductivity. It is obvious that the electrical conductivity significantly increases with the substitution of Bi atoms by Sb atoms. It is well-known that when $AgBiSe_2$ crystallizes in the cubic phase, a NaCl-type structure with Ag and Bi ions is distributed statistically between the close packed layers of selenium ions.[13] Because of the disordered arrangements of Ag and Bi in the lattice of the cubic phase, $AgBiSe_2$ is found to behave in a metallic way.[14] In our study, nonambient cubic phase $AgBiSe_2$ was stabilized to room temperature because of the formation of solid solution by the incorporation of Sb into the lattice. So, the significant increase in electrical conductivity should be an inevitable result of the formation of a solid solution, which at the same time plays an important role in the stabilization of nonambient high temperature phase at room temperature.

The thermal conductivities of $AgBiSe_2$ and $AgBi_{0.5}Sb_{0.5}Se_2$ solid-solutioned nanoplates are displayed in Figure 5c. As shown in Figure 5c, the thermal conductivity of Sb substituted samples is significantly lower than that of $AgBiSe_2$ in the whole measured temperature range. At room temperature, the thermal conductivity of $AgBi_{0.5}Sb_{0.5}Se_2$ solid-solutioned nanoplates is 0.26 W/mK, which is much lower than that of $AgBiSe_2$ (0.45 W/mK). This significant reduction of thermal conductivity can be synergistically attributed to the disordering, point defects, and nanostructures. On the one hand, because of the substitution of Bi atoms by Sb atoms, the high temperature cubic phase is stabilized to room temperature through the formation of solid solution. In the cubic phase, the ultralow thermal conductivity was intrinsically limited by phonon−phonon umklapp and normal processes, which arise due to strong anharmonicity of the bonding arrangement in this compound.[11] On the other hand, the solid solutions provide an environment of atomic mass fluctuation throughout the crystal lattice (i.e., disorder) and introduce more point defects. Atomic substitutions in solid solution can scatter short-wavelength phonons due to the differences in mass;[22] thus, disorder of the crystal lattice and point defect scattering serves to decrease the lattice thermal conductivity by increasing the frequency and magnitude of the scattering events for the heat carrying phonons. Moreover, the nanostructures of the $AgBi_{1-x}Sb_xSe_2$ nanoplates serve to introduce a large density of interfaces in which long-wavelength phonons can be effectively scattered. So, in our study, the ultralow thermal conductivity was obtained, which is very beneficial to obtain high *ZT* value. According to the measured electrical conductivity, Seebeck coefficient, and thermal conductivity, the *ZT* values were calculated and plotted as a function of temperature in Figure 5d. Obviously, the *ZT* values of $AgBi_{0.5}Sb_{0.5}Se_2$ are higher than those of $AgBiSe_2$ in the whole measured temperature range (300−550 K) because of significantly increased electrical conductivity and decreased lattice thermal conductivity through the formation of solid solution by Sb atoms substituted Bi atoms.

To further lower the thermal conductivity, it is necessary to scatter the phonon in the whole wavelength. From this point of view, homojunctions are constructed with the same building blocks of nanoscale dimensions, and can provide a lot of interfaces similar to heterojunctions for the reduction of thermal conductivity, while they do not deteriorate the electrical conductivity simultaneously because of their homogeneous compositions. Therefore, inspired by the potential advantages of homojunctions, we synthesized the solid-solutioned homojunctions in $AgBi_{0.5}Sb_{0.5}Se_2$ nanoplates as an example. The structure and morphologies of the as-prepared $AgBi_{0.5}Sb_{0.5}Se_2$ solid-solutioned homojunction nanoplates were extensively characterized by XRD, FESEM, HRTEM, and SAED measurements. As shown in Figure S3a, the series of Bragg reflections in the XRD patterns of $AgBi_{0.5}Sb_{0.5}Se_2$ solid-solutioned homojunction nanoplates can be perfectly identical to the previous $AgBi_{0.5}Sb_{0.5}Se_2$ solid-solutioned nanoplates without homojunction, which indicates that the formation of homogeneous structure does not affect the crystal structure of the samples. No other peaks are observed belonging to impurities, such as Ag, Ag_2Se, or other compounds. Figure 4d shows the high-magnification FESEM images (low-magnification are shown in Figure S3b in the Supporting Information) of the as-obtained $AgBi_{0.5}Sb_{0.5}Se_2$ solid-solutioned homojunction nanoplates. It is evident that the platelike nanostructures are dominant while many small particles adhering on the surface of nanoplates compared to the $AgBi_{0.5}Sb_{0.5}Se_2$ solid-solutioned nanoplates with smooth surface. In addition, as seen in Figure 4d, no evident changes of the edge length and thickness of the nanoplates were observed. Figure 4e is a lattice-resolved HRTEM image taken from the contact area of the particle and surface of the nanoplate. It can be seen that the lattice fringes extend through the particle and surface of the nanoplate without interruption by any visible boundaries. The well-resolved 2D lattice fringes show that the nanoplate is a well-crystallized single crystal. The plane spacings of 2.910 Å correspond to the lattice planes of (200). Figure 4f shows the SAED pattern of the contact area of the particle and surface of the nanoplate, which displays only one set of reciprocal spots also show the single-crystal nature of the fusion region.

Corresponding to the front FESEM and HRTEM examination, we can clearly see that the formation of the homojunction makes the originally smooth surface of solid-solutioned nanoplates become very rough. Rough surfaces are expected to make an additional contribution toward improving the thermoelectric properties.[23,24] The temperature dependence of the thermoelectric property for $AgBi_{0.5}Sb_{0.5}Se_2$ solid-solutioned homojunction nanoplates is shown in Figure 5. As seen from

dx.doi.org/10.1021/ja3020204 | J. Am. Chem. Soc. 2012, 134, 7971−7977

Figure 5, there is no significant Seebeck coefficient (Figure 5a) and electrical conductivity (Figure 5b) change between the nanoplates with smooth and rough surfaces, while the thermal conductivity (Figure 5c) has significantly reduced in the whole measured temperature range. The thermal conductivity of $AgBi_{0.5}Sb_{0.5}Se_2$ solid-solutioned homojunction nanoplates is 0.18 W/mK at room temperature and 0.14 W/mK at 550 K, respectively, which is much lower than that of $AgBi_{0.5}Sb_{0.5}Se_2$ solid-solutioned nanoplates with smooth surface (0.26 W/mK at room temperature and 0.21 W/mK at 550 K, respectively). That is to say, the thermal conductivity has reduced by 31% at room temperature and 33% at 550 K, respectively. As known, the thermal conductivity (κ) is the sum of two independent components, a lattice contribution κ_l, and an electronic contribution κ_e. In this case of the homojunction formation, the reduction of total thermal conductivity can be much attributed to the reduction of the lattice thermal conductivity (κ_l) rather than the electronic thermal conductivity (κ_e) because of the almost no changed electrical conductivity. It is well-known that phonons in a material have a spectrum of wavelengths and phonons with different wavelengths are subordinate to different phonon scattering mechanisms. While the point defects in solid solution strongly scatter the short-wavelength phonons, and the grain boundary of nanostructures strongly scatter long-wavelength phonons, the surface roughnees scattering dominates in the mid-wavelength region.[25,26] Therefore, in this study, the rough surface introduced by the formation of solid-solutioned homojunciton nanoplates may efficiently scatter the nearly full wavelength phonons (see Scheme 1). As a result, significant reduction in lattice thermal conductivity was achieved in solid-solutioned homojunction samples, and the *ZT* value was significantly enhanced. As seen in Figure 5d, the *ZT* value of solid-solutioned $AgBi_{0.5}Sb_{0.5}Se_2$ homojunction nanoplates was further increased to 1.07 at 550 K.

Scheme 1. Schematic Diagram Illustrating Various Phonon Scattering Mechanisms in $AgBi_{0.5}Sb_{0.5}Se_2$ Solid-Solutioned Homojunction Nanoplates

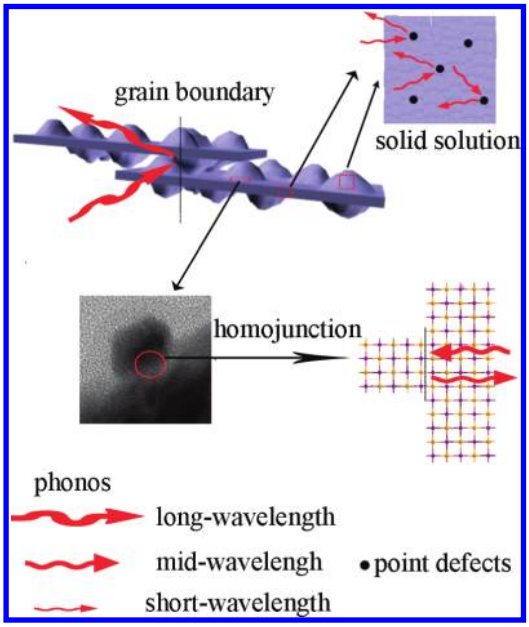

CONCLUSION

In conclusion, we first highlight the formation of solid-solutioned homojunctions in high temperature phase with disordered lattices as a novel and effective way to optimize the low/mid-temperature thermoelectric property. The two strategies of formation of solid solution and homojunctions in lattice disordering compound independently and effectively prevent the deterioration of electrical conductivity while thermal conductivity can be suppressed, comparing to conventional solid-solutioned and heterojunction strategies. As an example, the substitution of Sb in the lattice frameworks successfully stabilized the nonambient cubic $AgBiSe_2$ phase to room temperature through the formation of $AgBi_{1-x}Sb_xSe_2$ solid solution, which shows desirable low/mid-temperature thermoelectric property. Because the disordered state was stabilized to room temperature, the high electrical conductivity and low thermal conductivity were both achieved in the whole temperature range, which leads to the improved thermoelectric performance in a wide working temperature range compared to the originally nonambient compounds. Furthermore, in situ formed homojuncitons on the surface of solid-solutioned nanoplates were also first achieved through a simple colloidal method. Along with the effective scattering of mid-wavelength phonons by the rough surface created by the formation of homojunction, $AgBi_{0.5}Sb_{0.5}Se_2$ solid-solutioned homojunction nanoplates show much lower thermal conductivity with no deteriorated electrical conductivity. Of note, the perfect "phonon glass electron crystal" (PGEC) materials, which possess both high electrical conductivity and low thermal conductivity, have not been acquired yet. Our findings reveal that the formation of a solid solution coupled with homojunctions allows synergistically much enhanced thermoelectric properties through the significant reduction of thermal conductivity with no deteriorated electrical conductivity, which may conform the "PGEC" approach.

ASSOCIATED CONTENT

Supporting Information

Survey XPS spectra for $AgBi_{1-x}Sb_xSe_2$ solid-solutioned nanoplates. XRD patterns and FESEM images of $AgBi_{0.5}Sb_{0.5}Se_2$ solid-solutioned nanoplates before and after surfactant removal and hot-pressing. XRD patterns and low-magnification FESEM image for $AgBi_{0.5}Sb_{0.5}Se_2$ solid-solutioned homojunction nanoplates. This material is available free of charge via the Internet at http://pubs.acs.org.

AUTHOR INFORMATION

Corresponding Author

yxie@ustc.edu.cn

Notes

The authors declare no competing financial interest.

ACKNOWLEDGMENTS

This work was financially supported by National Basic Research Program of China (No. 2009CB939901), National Natural Science Foundation of China (11079004, 90922016, 10979047, J1030412), and innovation project of Chinese Academy of Science (KJCX2-YW-H2O).

REFERENCES

(1) Heremans, J. P.; Jovovic, V.; Toberer, E. S.; Saramat, A.; Kurosaki, K.; Charoenphakdee, A.; Yamanaka, S.; Snyder, G. J. *Science* **2008**, *321*, 554.
(2) Johnsen, S.; He, J. Q.; Androulakis, J.; Dravid, V. P.; Todorov, I.; Chung, D. Y.; Kanatzidis, M. G. *J. Am. Chem. Soc.* **2011**, *133*, 3460.
(3) Yu, J.-K.; Mitrovic, S.; Tham, D.; Varghese, J.; Heath, J. R. *Nat. Nanotechnol.* **2010**, *5*, 718.
(4) Snyder, G. J.; Toberer, E. S. *Nat. Mater.* **2008**, *7*, 105.
(5) Fitsul, V. I. *Heavily Doped Semiconductors*; Plenum Press: New York, 1969.
(6) Slack, G. A. In *CRC Handbook of Thermoelectrics*; Rowe, D. M., Ed.; CRC Press: Boca Raton, FL, 1995, p 407.
(7) Nolas, G. S.; Morelli, D. T.; Tritt, T. M. *Annu. Rev. Mater. Sci.* **1999**, *29*, 89.
(8) Toberer, E. S.; May, A. F.; Snyder, G. J. *Chem. Mater.* **2010**, *22*, 624.
(9) Kleinke, H. *Chem. Mater.* **2009**, *22*, 604.
(10) Sabah, K. B.; Fleurial, J. P.; Richard, B. K. *Chem. Commun.* **2010**, *46*, 8311.
(11) Morelli, D. T.; Jovovic, V.; Heremans, J. P. *Phys. Rev. Lett.* **2008**, *101*, 035901.
(12) Manolikas, C.; Spyridelis, J. *Mater. Res. Bull.* **1977**, *12*, 907.
(13) Larson, P.; Mahanti, S. D. American Physical Society, Annual March Meeting, March 12−16, 2001.
(14) Lan, Y. C.; Minnich, A. J.; Chen, G.; Ren, Z. F. *Adv. Funct. Mater.* **2010**, *20*, 357.
(15) Liu, W. S.; Yan, X.; Chen, G.; Ren, Z. F. *Nano. Energy* **2011**, *1*, 42.
(16) Xia, H. X.; Luo, L.; Fraisse, G. *Renewable Sustainable Energy Rev.* **2007**, *11*, 923.
(17) Wan, C. L.; YifengWang, Y. F.; Wang, N.; Norimatsu, W.; Kusunoki, M.; Koumoto, K. *Sci. Technol. Adv. Mater.* **2010**, *11*, 044306.
(18) Whittaker, L.; Wu, T. L.; Stabile, A.; Sambandamurthy, G.; Banerjee, S. *ACS Nano* **2011**, *5*, 8861.
(19) Wu, C. Z.; Feng, F.; Feng, J.; Dai, J.; Peng, L. L.; Zhao, J. Y.; Yang, J. L.; Si, C.; Wu, Z. Y.; Xie, Y. *J. Am. Chem. Soc.* **2011**, *133*, 13798.
(20) Poudeu, P. F. P.; D'Angelo, J.; Huijun Kong, H. J.; Downey, A.; Short, J. L.; Pcionek, R.; Hogan, T. P.; Uher, C.; Kanatzidis, M. G. *J. Am. Chem. Soc.* **2006**, *128*, 14347.
(21) Shakouri, A. *Annu. Rev. Mater. Res.* **2011**, *41*, 399.
(22) Scheele, M.; Oeschler, N.; Meier, K.; Kornowski, A.; Klinke, C.; Weller, H. *Adv. Funct. Mater.* **2009**, *19*, 3476.
(23) Hochbaum1, A. I.; Chen, R. K.; Delgado, R. D.; Liang, W. J.; Garnett, E. C.; Najarian, M.; Majumdar, A.; Yang, P. D. *Nature* **2008**, *451*, 163.
(24) Martin, P. N.; Aksamija, Z.; Pop, E.; Ravaioli, U. *Nano Lett.* **2010**, *10*, 1120.
(25) Kim, H.; Park, Y. H.; Kim, I.; Kim, J.; Choi, H.; Kim, W. *Appl. Phys. A: Mater. Sci. Process.* **2011**, *104*, 23.
(26) Qiu, B.; Sun, L.; Ruan, X. L. *Phys. Rev. B* **2011**, *83*, 035312.